Predicting BVI Loadings and Wake Structure of the HART Ⅱ Rotor Using Adaptive Unstructured Meshes

Dong Ok Yu*, Mun Seung Jung* and Oh Joon Kwon**
Department of Aerospace Engineering, KAIST,
Daejeon 305-701, Korea

Yung H. Yu***
Department of Aerospace Engineering, Konkuk University,
Seoul 143-701, Korea

Abstract

The flow fields around the HART Ⅱ rotor were numerically investigated using a viscous flow solver on adaptive unstructured meshes. An overset mesh and a deforming mesh technique were used to handle the blade motion including blade deflection, which was obtain from the HART Ⅱ experimental data. A solution-adaptive mesh refinement technique was also used to capture the rotor wake effectively. Comparison of the sectional normal force and pitching moment at 87% radial station between the two cases, with and without the blade deflection, showed that the blade loading is significantly affected by blade torsion. It was found that as the mesh was refined, the strength of tip vortex is better preserved, and the magnitude of high frequency blade loading, caused by blade-vortex interaction (BVI), is further magnified. It was also found that a proper time step size, which corresponds to the cell size, should be used to predict unsteady solutions accurately. In general, the numerical results in terms of the unsteady blade loading and the rotor wake show good agreement with the experimental data.

Key Words : CFD(Computational Fluid Dynamics), Unstructured Overset Mesh Technique, Deforming Mesh Technique, BVI(Blade-Vortex Interaction), Blade Deflection

Introduction

For several decades, helicopters have been consistently designed with better performance and productivity as the major driving goal, and acoustic problems have not been the primary concern. However, recently, much effort has focused on reducing the noise of helicopters, as the community concern of the noise pollution and the military concern of stealth are increased. In helicopter aerodynamics, there are various types of noise sources, such as transmission engine noise, high speed impulsive noise created by the shock wave, and blade-vortex interaction (BVI) noise, etc. When BVI noise occurs, it is highly impulsive and generally dominates the other sources of noise. The strength of BVI noise is determined by a few parameters, such as the strength of the tip vortex, the crossing angle between the tip vortex and the blade, and the vertical distance from the tip vortex core to the blade. Among them, the vertical distance, which is called the miss distance, has the strongest influence on BVI noise, which depends on the

* Graduate Research Assistant
** Professor
E-mail : ojkwon@kaist.ac.kr Tel : +82-42-350-3720 Fax : +82-42-350-3710
*** Professor

flightcondition. When a helicopter operates in a descending flight condition, the upwash tends to convect the tip vortex into the rotor disc plane, and over a certain part of the disc, the blades travel close to the tip vortex. The rapid variation of the induced velocity associated with the tip vortex causes large time-varying fluctuation of loading at the leading edge region of the blade, which generates strong BVI noise.

To reduce this BVI noise, first of all, understanding the wake around the helicopter rotor should be achieved. There are several different types of computational methods for the rotor wake prediction, ranging from vortex wake method with a lifting line/surface model to computational fluid dynamics (CFD) solving the Euler/Navier-Stokes equations. Vortex wake method can be classified roughly into two types: a prescribed wake model [1] and a free wake model [2]. The prescribed wake model assumes a fixed wake geometry based on parameters such as the advanced ratio, thrust, etc. This simplifies the wake analysis and saves computation time. In the free wake model, the geometry of the wake is iteratively calculated at every time step using a local velocity including the components induced by the wake and the bound vortex. This model provides increased accuracy over the prescribed wake model when complex wake geometry evolves, such as in the transitional flight regimes. Although the vortex wake method can provide fairly accurate preliminary predictions of the wake and the blade loading, there are inevitable limitations to these wake methods, due to the simplification and the inadequacy involved in modeling a real flow. In contrast, CFD has potential advantage for a detailed understanding of the wake around the helicopter rotor, but considerable computing power and memory are needed to capture the rotor wake accurately without numerical dissipation. Currently, CFD is widely utilized for predicting rotor wake, owing to the tremendous advancement of computers.

In the CFD calculations, three factors should be considered to predict the rotor wake accurately. First, an large number of grid points are required to prevent numerical dissipation. Second, the strength of the tip vortex must be accurately predicted. Finally, the position of the tip vortex must also be accurately predicted. Recent advances [3, 4] in coupling computational fluid dynamics (CFD) to computational structural dynamics (CSD) have demonstrated significant progress in meeting the last two requirements, which are directly related to the blade motion. Overall, results from the coupled CFD/CSD method show significant improvements for the prediction of the blade loading and the deflection over the traditional lifting-line models that are present in most helicopter comprehensive codes. However, there are still several problems, which are not clearly identified, because of the extensive error range in CFD/CSD coupling analyses. Recently, a decoupled analysis is widely used to minimize these uncertainties. To decouple CSD from CFD, the blade deflection is prescribed from experimental data or predicted results from comprehensive rotor analysis tools. This approach is effective to inspect a CFD code prior to CFD/CSD coupling analysis [5].

In the present study, viscous flow simulation of the HART Ⅱ rotor blade was performed to investigate the rotor wake and the blade loading. Information about the blade motion including blade deflection was obtained from the HART Ⅱ experimental data. As a mesh deformation technique, a spring analogy and an algebraic method were used. A solution-adaptive mesh refinement technique was also used to capture the rotor wake effectively. To investigate the effect of the blade deflection on the blade loading, calculations were performed for two cases with and without blade deflection. Additionally, calculations were performed to investigate the effect of grid density and time step size on the blade loading and the rotor wake. For validation, the predicted results are compared with existing experimental data.

HART Ⅱ Test

The HART Ⅱ (Higher Harmonic Control Aeroacousic Rotor Test Ⅱ) experiment[6, 7] used a 40% Mach-scaled, four-bladed, hingeless BO105 model rotor. The rotor blades are rectangular with -8° linear twist angle and a precone angle of 2.5°. The blade features a modifiedNACA23012 airfoil with a trailing-edge tab of 5.4 mm length and 0.8 mm thickness. The rotor was installed with the rotor shaft angle of 5.3 deg (nose-up) that was designed to simulate descending flight. For the computation, the rotor shaft angle of 4.5 deg was used for the correction of the wind

Table 1. HARTⅡ test conditions

Rotor radius	2.0(m)
Blade chord length	0.121(m)
Twist angle	-0°.8
Precone angle	2°.5
Thrust coefficient	0.0044
Inflow ratio	0.15
Shaft angle	4°.5
Tip Mach number	0.6387

tunnel wall effects. Three different cases were tested: a baseline(BL) case with conventional control input, and two other cases with higher harmonic control(HHC) inputs, called as minimum-noise(MN) and minimum vibration(MV) cases. In the present work, only the BL case was studied. The test conditions are summarized in Table 1.

Numerical Method

In the present study, an unstructured mesh CFD flow solver [8, 9] was used for the simulation of time-accurate viscous flows around the HARTⅡ rotor. The governing Reynolds-Averaged Navier-Stokes equations were discretized using a vertex-centered finite-volume method. The flow domain was divided into a finite number of control volumes composed of median duals surrounding each vertex. The inviscid flux terms were computed using Roe's flux-difference splitting scheme. The flow variables at each dual face were computed by using a linear reconstruction approach for second-order spatial accuracy. The second-order derivatives of the viscous terms are evaluated by the Green-Gauss theorem, and the viscous flux terms was computed by adopting a modified central differencing. An implicit time integration algorithm based on a linearized second-order Euler backward difference was used to advance the solution in time. The linear system of equations was solved at each time step using a point Gauss-Seidel method. The Spalart-Allmaras one-equation turbulence model was used to estimate the eddy viscosity. In order to reduce the large computational time, a parallel algorithm based on a domain decomposition strategy was adopted. The load balancing between processors was achieved by partitioning the global computational domain into local subdomains using the MeTiS libraries. The Message Passing Interface was used to transfer the flow variables across the subdomain boundaries. All calculations were performed on PC-based Linux clusters.

Blade Deflection

In the present study, the blade motion was prescribed, based on a variable-separable interpolation of the blade deflections that were measured at discrete azimuthal and radial locations on each blade. Each component D of the deflection is reconstructed using the interpolating function,

$$D(r,\psi) = \sum_{i=1}^{N_r} \sum_{j=1}^{N_a} a_{ij} R_i(r) P_j(\psi) \tag{1}$$

where r is the non-dimensional radial coordinate, and ψ is the azimuth angle. N_r and N_a are respectively the number of radial and azimuthal interpolation functions, $R_i(r)$ and $P_j(\psi)$, used todescribed the blade deflection. The radial interpolation functions were taken to be polynomials, and the azimuthal interpolation functions were taken to be the components of a Fourier series,

$$R_i(r) = r^{i-1} \tag{2}$$

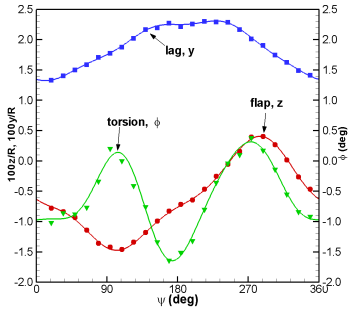

(a) Time history at r/R=1

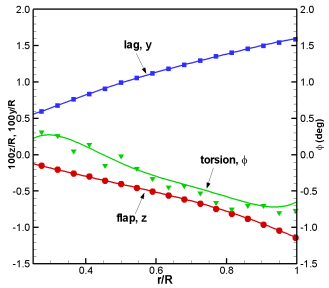

(b) Radial distribution at ψ=64

Fig. 1. Comparison of the blade deflection between the approximation(line) and measurement(symbol)

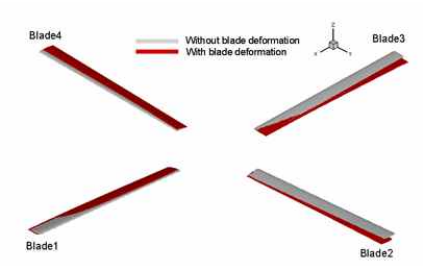

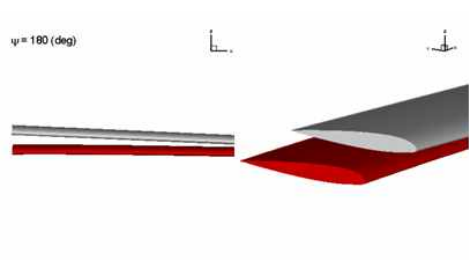

Fig. 2. Comparison of the blade motion between with and without blade deflection

$$P_j(r) = \begin{cases} \cos\dfrac{j-1}{2}\psi & \text{if } j\in(1,3,5.....) \\ \sin\dfrac{j}{2}\psi & \text{if } j\in(2,4,6.....) \end{cases} \quad (3)$$

The coefficients a_{ij} of the interpolation function were obtained using a simple least squares fitting, and the set of coefficients are given in Ref. 10. In Fig 1, the approximations of the blade deflection are compared with the measured data. The maximum differences between the approximation and measurement are 0.5° and 0.5 mm for the torsion and flap/lag, respectively [10]. Finally, to simulate the blade elastic motion, the grid points on the blade surface were moved using the position of the quarter chord line, and the results are shown in Fig 2.

Computational Mesh

In the present study, an unstructured overset mesh technique [11] was used to simulate the relative motions of the blades. In this overset mesh scheme, the total mesh topology was composed of multiple independent mesh blocks: main background mesh representing the complete computational domain, and sub-block meshes surrounding each individual blade. To capture the boundary layer on the blade and the shear flow in the near-field wake region, a hybrid meshtopology containing both prismatic and tetrahedral cells is used. Fig. 3 shows the overset mesh system and the hybrid mesh topology on the blade surface. Deforming meshes are used in many computational applications, including problems with deforming boundaries and interface. A common technique to deform a mesh is the spring analogy [12]. In the present study, a ball-vertex spring analogy [13] was adopted for inviscid elements for the robustness, and an algebraic method [14] based on the basis decomposition of normal edge vectors was used for the deformation of viscous elements. A solution-adaptive mesh refinement technique was applied to better resolve the tip vortex in the wake. In the present study, a quasi-unsteady mesh refinement

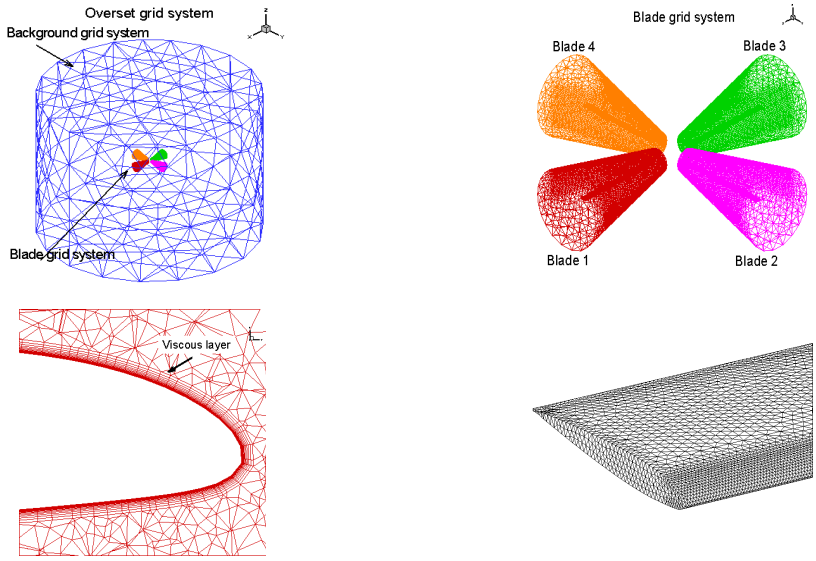

Fig. 3. Hybrid overset mesh and surface triangulation

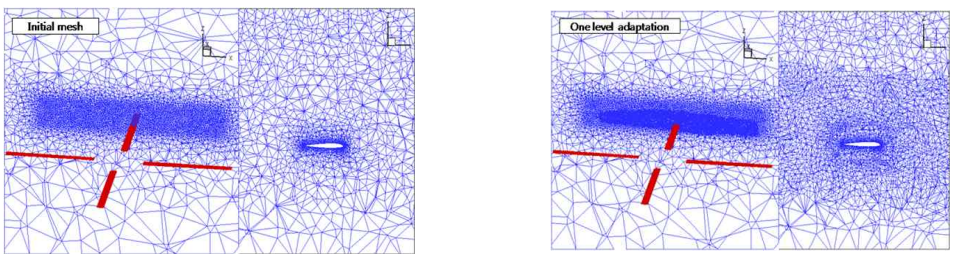

Fig. 4. Initial coarse mesh and mesh after one level adaptation

technique was adopted to avoid excessive computational time required by dynamic mesh adaptation applied in a fully unsteady manner. As the blades rotated, cells having high vorticity were tagged at every time step. Once the rotor completed one period of rotation, the calculation was paused and the mesh adaptation was applied. The initial mesh consisted of 2,897,615 nodes and 9,043,187 cells. The typical grid size in the wake region corresponds to 0.25c, where c is chord length. After one level of mesh adaptation, the number of nodes and cells increased to 4,451,881 and 18,210,699, respectively. In Fig. 4, it is shown that the initial mesh before mesh adaptation is very coarse, which may not be appropriate for preserving the tip vortex. The relative size of the cells decreased after mesh adaptation. The flow was set to be the free streamvalue at the inflow boundary. The no-slip condition was applied at the blade surface, and the characteristic boundary condition with Riemann invariants was set at the far-field boundary.

Result and Discussion

As mentioned earlier, in the present study, viscous flow simulation for the BL case of HARTII rotor blade was conducted to investigate the blade loading and the rotor wake. Sectional normal force and pitching moment, C_nM^2 and, C_mM^2 defined in Eq. (4) and (5), were calculated at 87% radial station, and the trajectory of the tip vortex in the wake region was also observed.

$$C_nM^2 = \frac{2}{pa_\infty^2 c}\left(\sum_{low} P_{low}\triangle x_{low} - \sum_{up} P_{up}\triangle x_{up}\right) \tag{4}$$

$$C_m M^2 = \frac{2}{p a_\infty^2 c^2}\left(\sum_{low} P_{low} \triangle x_{low} x_{low} - \sum_{up} P_{up} \triangle x_{up} x_{up}\right) \quad (5)$$

Effect of blade deflection

To investigate the effects of blade deflection on the blade loading, two cases, with/without blade deflection, were simulated. The predicted results, aerodynamic coefficients, $C_n M^2$ and $C_m M^2$ were compared with existing experimental data in Fig. 5. In the experimental data, fluctuations of the blade loading, caused by BVI, are shown at the rear of rotor disc. However, this high frequency blade loading does not appear in both of the two cases. This is because the simulations were conducted on the initial coarse mesh, and thus the tip vortex was not preserved well due to numerical dissipation. Although the fluctuating blade loading is not presented in the present results with blade deflection, the results show good agreement with the low frequency component of the blade loading measured in the experiment, particularly at the retreating side. The discrepancies at the advancing side may be attributed to the inaccurate blade motion due to the missing experimental data for the blade deflection around 0° and 180° azimuth angles. The large difference between with and without blade deflection is shown at the front of the rotor disc. Thetendency of this difference is also shown in the blade torsion in Fig. 1(a), which is directly related to blade loading. Therefore, it is obvious that the blade deflection has non-negligible influence on the blade loading, and thus to predict the blade loading accurately, the blade deflection must be considered properly.

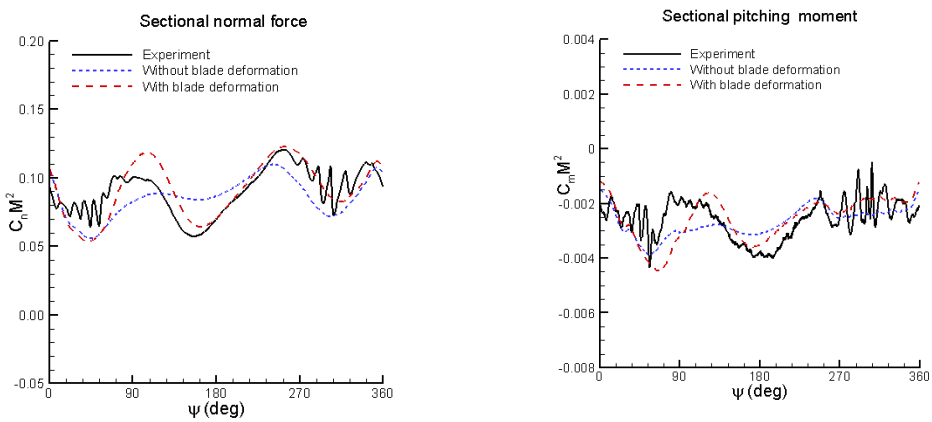

Fig. 5. Effect of blade deflection on aerodynamic force coefficients, $C_n M^2$ and $C_m M^2$, at 87% radial station

Effect of grid density

In this study, a solution-adaptive mesh refinement technique was adopted to investigate the effect of grid density on the blade loading and rotor wake. Additionally, $C_n M^2$ and $C_m M^2$ data were filtered to distinguish high frequency components from low ones. In Fig. 6, the predicted results for the high and low frequency components of $C_n M^2$ were compared with the experimental data. The high frequency loading is exclusively associated with BVI, while the low frequency loading is primarily associated with control pitch input angles and the deflection of the blade. Therefore, in analyzing the characteristics of the blade loading, it is effective to separate the full signal data into the low and high frequency components. As the computational mesh was refined further, the magnitude of the high frequency loading was also amplified. However, the low frequency component was independent to mesh refinement. In Fig. 7, $C_m M^2$

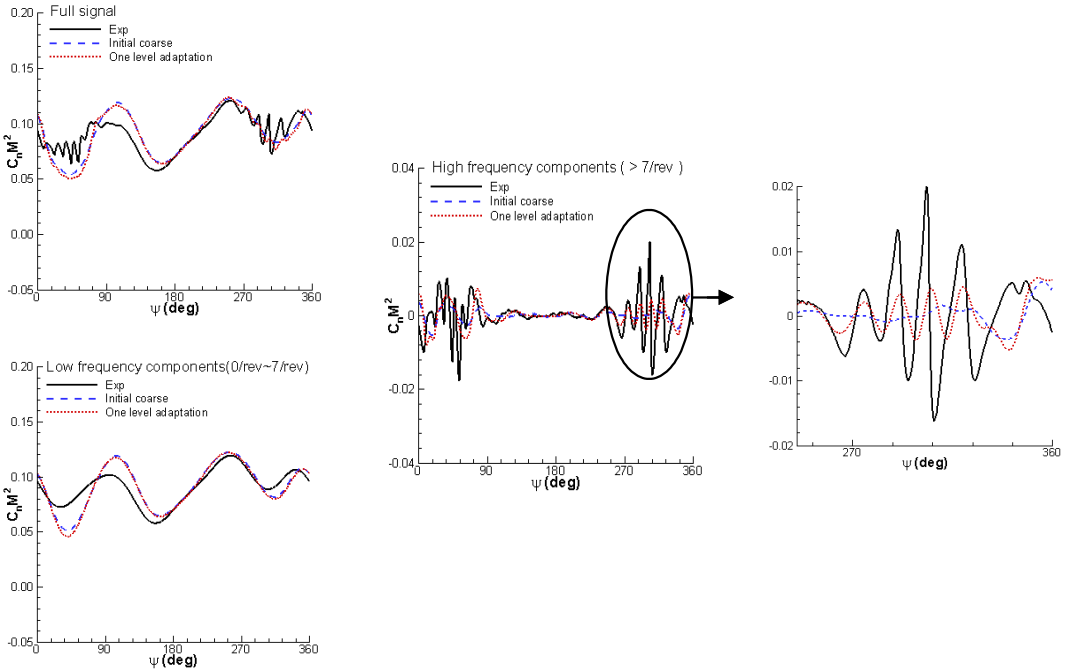

Fig. 6. Effect of grid density on sectional normal force coefficient, C_nM^2 at 87% radial station

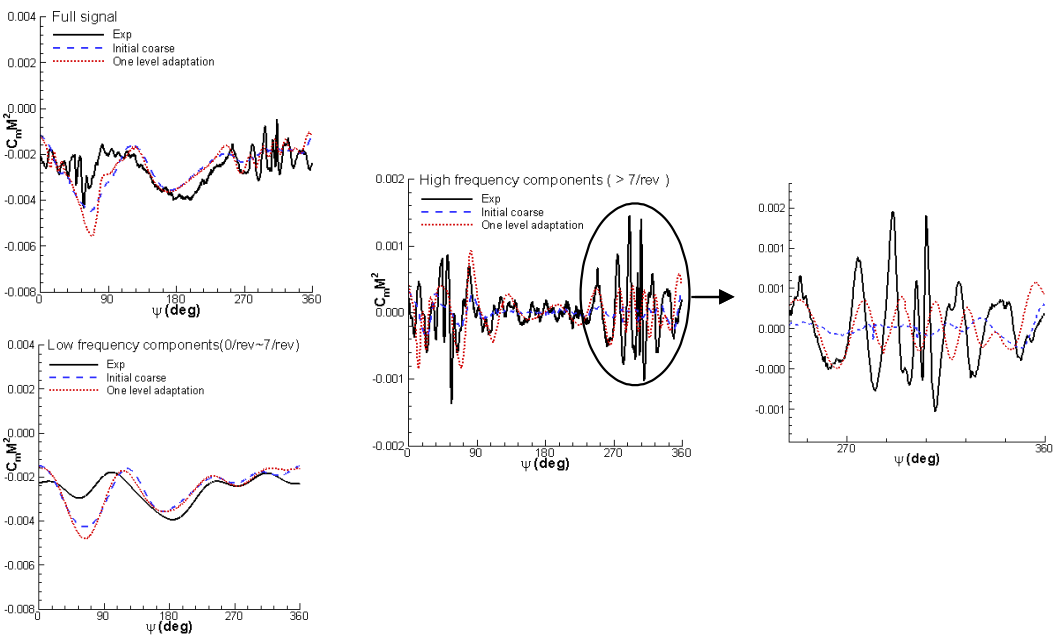

Fig. 7. Effect of grid density on sectional pitching moment coefficient, C_mM^2 at 87% radial station

shows the same tendency as C_nM^2in Fig. 6. As shown in Fig. 8, the tip vortex generated at the front of the rotor disc, was highly dissipated on the initial coarse mesh. After one level of mesh adaptation, the strength of the tip vortex was better preserved than that of the initial coarse mesh, but is still not enough to capture the realistic BVI phenomenon in the HARTⅡ experiment.

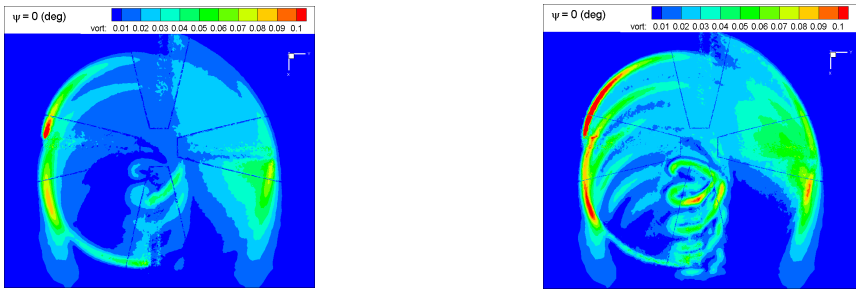

(a) Initial mesh (b) One level adaptation

Fig. 8. Effect of grid density on iso-vorticity contours

Effect of time step size

In CFD calculations, time step size is one of the most fundamental parameters to obtain accurate unsteady solutions. When smaller time step size is used, more accurate unsteady solution can be achieved, but the computational time becomes lager. In this study, time step size was tested to validate the present results and to find a compromise between solution accuracy and computational time. Four different time step sizes, 1.0°, 0.5°, 0.25° and 0.125°, were used for this test. As shown in Fig. 9, non-physical oscillation of the blade loading is observed for the two cases, 1.0° and 0.5° time step size, due to numerical errors, while the blade loading is independent on the time step size, when the size is smaller than 0.25°. In Fig. 10, iso- vorticity contours show a similar tendency with the blade loading. For the time step size from 0.5° to 1.0°, it is shown that vorticity contours largely vary for the time step size, but are converged in the case of the size smaller than 0.25°. From these results, in this study, time step size of 0.25° was used.

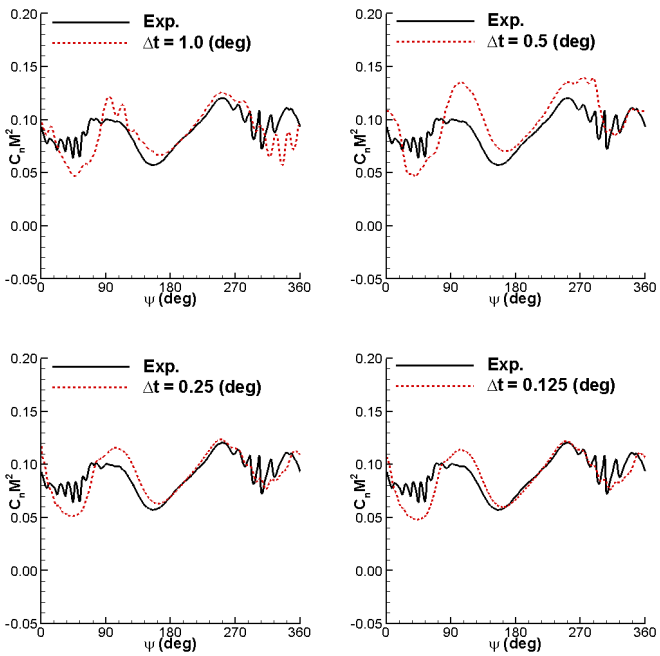

Fig. 9. Effect of time step size on sectional normal force coefficient, C_nM^2, at 87% radial station

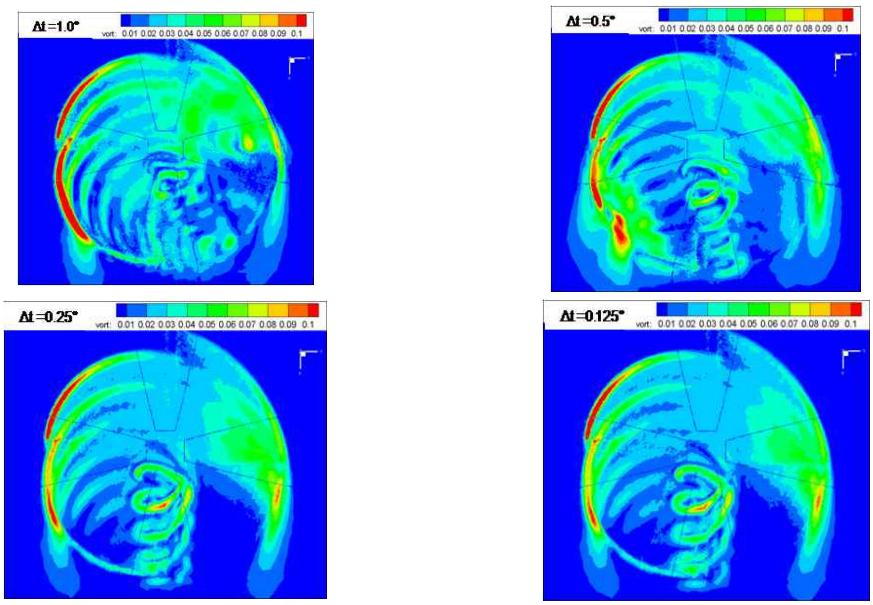

Fig. 10. Effect of time step size on iso-vorticity contours

Vortex position

In Fig. 11, instantaneous wake structures, at the azimuth of 20°and 70°, are compared between the present calculation and the experiment in a plane view. The predicted wake geometry is shown to match closely to the experimental data. However, the tip vortex is gradually faded, due to numerical dissipation, and then disappears after all. Also, because the blades were modeled as finite wings with root cut-out for the computation, relatively strong root vortices develop. These root vortices are non-physical, and as a result, inaccurate prediction of the blade loading may be produced.

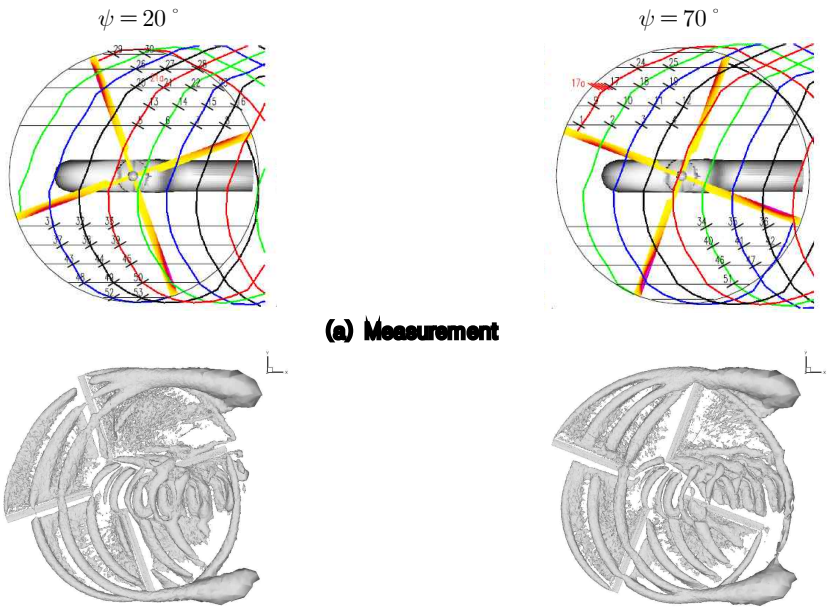

(a) Measurement

(b) Computation

Fig. 11. Measured and computed wake structure in a plane view

To investigate details of the trajectory of the tip vortex, Fig. 12 shows contour plots of the vorticity magnitude on two longitudinal slices located at 0.7R from the rotor hub, one at the advancing side of the rotor and the other at the retreating side. In this figure, the experimentally measured positions of the vortex cores are plotted as squares(azimuth angle, 20°) and circles(azimuth angle, 70°), and are labeled with a position corresponding to the location of the plane view in Fig. 11. In the hub coordinate system, z/R is positive in the upward direction and x/R is positive aft. The predicted result of the position of the tip vortex at the retreating side shows good agreement with that of the experiment, while at the advancing side, the results are slightly over-predicted. This is because the blade motion may be simulated inaccurately, due to the missing experimental data for the blade deflection around 0° and 180° azimuth angles.

In Fig. 13, pressure difference ($\triangle P = P_{up} - P_{low}$) on the blade leading edge is compared between the present computation and the experiment. The lower and upper surface pressures are given at 3% chordwise position of the blade, and the pressure difference is plotted both spanwisely and azimuthwisely for one rotor revolution. In the experiment data, the stripe patterns at the rear of the rotor disc, which represent fluctuations of the blade loading due to BVI, areobserved obviously. However, in the predicted results after mesh adaptation, these patterns are not well captured.

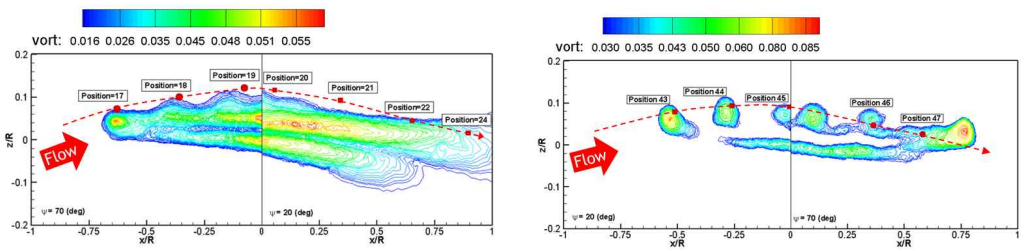

(a) y/R= 0.7 (b) y/R= - 0.7

Fig. 12. Tip vortex trajectory on the longitudinal slice (symbol:measured, contour:computed)

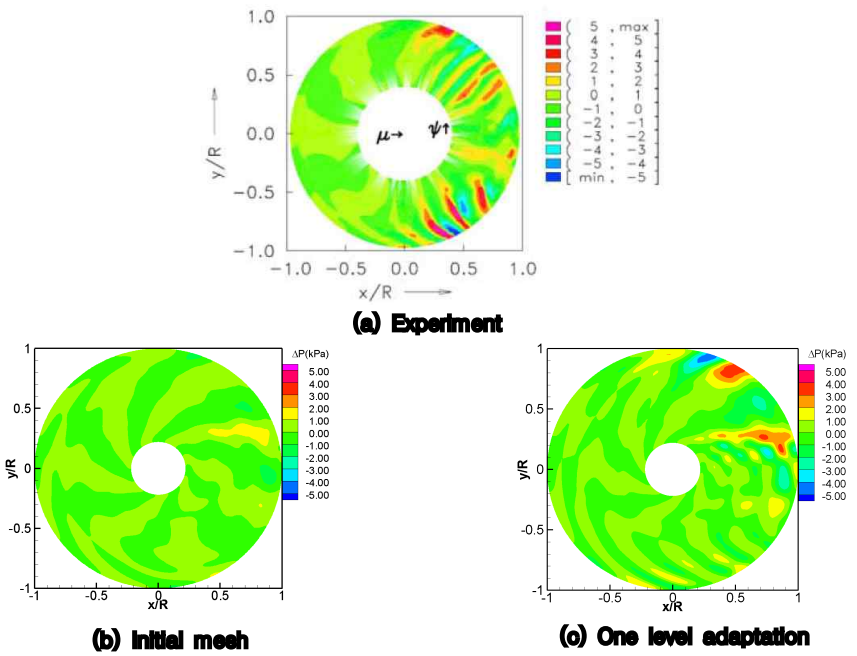

(a) Experiment

(b) Initial mesh (c) One level adaptation

Fig. 13. Leading edge pressure difference for one rotor revolution

Conclusions

In the present study, numerical simulation of viscous flows for the HARTII rotor blade was performed to investigate the blade loading and the rotor wake. A quasi-unsteady solution adaptive mesh refinement technique was used for the much accurate prediction of the tip vortex in the wake region without numerical dissipation. An unstructured overset mesh technique was adopted to simulate the rigid motion of the blade, and the mesh deformation due to blade deflection was taken care of by using a spring analogy and an algebraic method at every time step. The predicted results, in general, show good agreement with the existing experimental data. By comparing the normal force and pitching moment at 87% radial station between with and without the blade deflection, it was found that the blade loading is largely affected by the blade torsion. It was also found that a proper time step size, which corresponds to the cell size, should be used to obtainacurate unsteady solutions, such as the high frequency loading. As the initial mesh was refined, the strength of tip vortex was better preserved, and the magnitude of high frequency blade loading was further magnified. It was found that the present CFD solver with overset mesh and mesh deformation technique seems to perform well for the aeroelasticity analysis with CFD/CSD coupling.

Acknowledgement

This work is the outcome of a Manpower Development Program for Energy & Resources supported by the Ministry of Knowledge and Economy(MKE)

References

1. A. J. Landgrebe, “An Analytical Method for Predictiong Rotor Wake Geometry”, Journal of the American Helicopter Society, Vol. 14, No. 4, 1969.

2. W. Johnson, “Wake Model for Helicopter Rotor in High-Speed- Flight”, NASA Contractor Report, No. 177507, 1988.

3. A. Datta, J. Sitaraman, I. Chopra, and J. D. Baeder, “CFD/CSD Prediction of Rotor Vibratory Loads in High-Speed Flight”, Journal of Aircraft, Vol. 43, No. 6, 2006.

4. J. W. Lim, T. A. Nygaard, R. Strawn, and M. Potsdam, “Blade -Vortex Interaction Airloads Prediction Using Coupled Computational Fluid Structural Dynamics”, Journal of the American Helicopter Society, Vol. 2, No. 4, 2007.

5. C. M. Yang and T. Aoyama, “Effect of Computation Parameters on BVI Noise Prediction Using HARTII Motion data”, 34th European Rotorcraft Forum, 2008.

6. B. van der Wall, “2nd HHC Aeroacoustic Rotor Test (HARTII) - Part I: Test Documentation - “, DLR 1B 111-2003/21, Braunschweig, Germany, 2003.

7. B. van der Wall and C. Burley, “2nd HHC Aeroacoustic Rotor Test (HARTII) - Part II: Representative Results - “, DLR 1B 111-2005/3, Braunschweig, Germany, 2005.

8. M. S. Jung, O. J. Kwon and H. J. Kang, “Assessment of Rotor Hover Performance Using a Node-Based Flow Solver”, KSAS International Journal, Vol. 8, No. 2, 2007.

9. H. J. Kang and O. J. Kwon, “Unstructured Mesh Navier-Stokes Calculations of the Flow Field of a Helicopter Rotor in Hover”, Journal of American Helicopter Society, Vol. 47, No. 2, 2002.

10. M. Kelly, K. Duraisamy, and R. Brown, “Predicting Blade Vortex Interaction, Airloads and Acoustics using the Vorticity Transport Model”, Proceedings of the American Helicopter Society 9th Aeromechanics Specialist Meeting, San Francisco, USA, 2008.

11. M. S. Jung and O. J. Kwon, “A Parallel Unstructured Hybrid Overset Mesh Technique for Unsteady Viscous Flow Simulations”, International conference on Parallel computational fluid dynamics, Antalya, Turkey, 2007.

12. J. T. Batina, “Unsteady Euler Algorithm with Unstructured Dynamic Mesh for Complex-Aircraft Aerodynamic Analysis”, AIAA Journal, Vol. 29, No. 3, 1991.

13. C. L. Bottasso, D. Detomi, and R. Serra, “The Ball-vertex Method: A New Simple Spring Analogy Method for Unstructured Dynamic Meshes”, Computer Methods in Applied Mechanics and Engineering, Vol. 197, 2005.

14. D. B. Kholodar, S. A. Morton and R. M. Cummings, “Deformation of Unstructured Viscous Grids”, AIAA paper, 2005-0926.